韓國海洋工學會誌 第11卷 第4號, pp.130~140, 1997. 11

◉ 論 文

Experimental and Computational Investigation of the Flow around a Circular Cylinder

Mu-Seok Song* · Geun-Tae Yim** · Wu-Joan Kim**

(97년 8월 29일 접수)

실험 및 중첩격자를 이용한 수치해석에 의한 원형단면체 주위의 유동고찰

송 무 석* · 임 근 태** · 김 우 전**

Key Words : circular cylinder(원형단면체), vortex shedding(와류박리), pressure measurement (압력계측), flow visualization(유동 가시화), NS-equation, composite grid(중첩격자)

초 록

원형주상체 주위의 유동을 규명하기 위해 회류수조에서 원주방향으로 24개의 위치에 대하여 압력을 계측하였으며, laser sheet을 이용하여 유동을 가시화 하였다. Reynolds수가 4800에서 40000인 범위에 대하여 실험을 수행하였다. 또한, 원형단면체 주위의 비정상 층류유동에 대한 Navier-Stokes방정식의 해를 구하는 수치해석기법을 개발하였다. 효과적인 격자배치를 위하여 H와 O-type의 중첩격자를 사용하였고, 이산화 방법으로는 정규격자시스템에서 유한차분법을 적용하였다. 실험과 수치해석결과에서 뚜렷한 와류박리현상을 볼 수 있었으며, 압력계수(C_p), 항력계수(C_D), 스트로얼수(St)를 정량적으로 비교하였을 때, 비교적 잘 일치하는 것을 확인하였다.

1. INTRODUCTION

Although the flow around a circular cylinder seems to have become a textbook problem already, still many new researches treat the problem to verify their experimental and numerical tools. Moreover an increasingly popular usage of circular cylinders in offshore structures demands for more thorough understanding involved in the problem. When we think of an offshore floating structure moored by cables it undergoes relatively large excursive motion at relatively low frequencies, then the cable's viscous damping is said to be very important

* 홍익대학교 조선해양공학과
** 선박해양공학연구센터

to predict such motions precisely (Faltinsen[1990, 1993]). Partial treatment of such related problems has been performed by Suhara and Koteryama group (most of the reports are in Japanese), Bruce[1993], Hu et al.[1993] and Sibetheros[1993] if naming a few but still more reliable information is required.

Bearing the above in mind we established flow visualization tools and a numerical method can be used for such problems. The scope of the present work is not extended to the aforementioned such problems though, but we treated the flow around a circular cylinder exposed in a uniform stream.

The speed of the uniform flow is varied from 0.13m/s to 1.03m/s and the corresponding Reynolds numbers are 4850 and 39400, respectively. The flow is investigated by observing visualized images captured utilizing laser sheet and emitting particles seeded in the flow and by measuring pressure along the circumference of the cylinder.

The main difficulty in calculating unsteady incompressible flows arises from the fact that the continuity equation is a constraint to be imposed to obtain a divergence-free velocity field. In the present work a numerical method that solves the unsteady Navier-Stokes equations using the pressure-Poisson method, based on finite-difference schemes in a collocated composite overlaying grid system, is developed. The time-accurate solution was sought for the flow around a circular cylinder and the results are compared with the experiments.

2. EXPERIMENTS

2.1 EXPERIMENTAL SETUP

The CWC used in the experiment has a test section 1.5m long, 0.5m wide and 0.4m deep. It utilizes one impeller for the speed control and the maximum speed uniform enough was measured 1.1m/s. The turbulent intensity was not considered while the flow uniformity was verified by measuring the flow speed with Pitot tubes 5cm apart from CWC walls. From now on the flow speed is often referred as the corresponding CWC impeller frequencies.

Figure 1 shows the experimental setup for the flow visualization. The circular cylinder long enough to reach the tank bottom is fixed at the top. The free surface is covered with a plastic plate to suppress possible free surface deformations; consequently the experimental condition is similar to a cavitation tunnel environment. The light source is 300mw Argon-Ion laser and the beam is directed toward the interested region by using two precision mirrors and a cylindrical lens. A chopper is located at the very front of the laser nozzle and the chopper RPM is controlled by a PC to give a proper exposure time.

The emitting particles used were PVC powder whose density was carefully chosen to be neutrally buoyant. The particles are slightly heavier than water though, but the convection speed used in the experiment was believed to be large enough to carry the particles in the laser sheet. The visualized flow patterns are captured by using CCD camera as well as still picture camera from the bottom of the channel. ASA 3200 Kodak TMAX films were used for the still pictures and the video images were stored in a VCR at a rate of 30 frames per second.

For the pressure measurements a similar experimental setup is constructed. The circular cylinder with 24 pressure taps of 1.5mm diameter is vertically located. The pressure tap configuration is shown in Figure 2 and the number zero hole is facing the incoming flow. 24 pressure taps are connected to a scanny valve

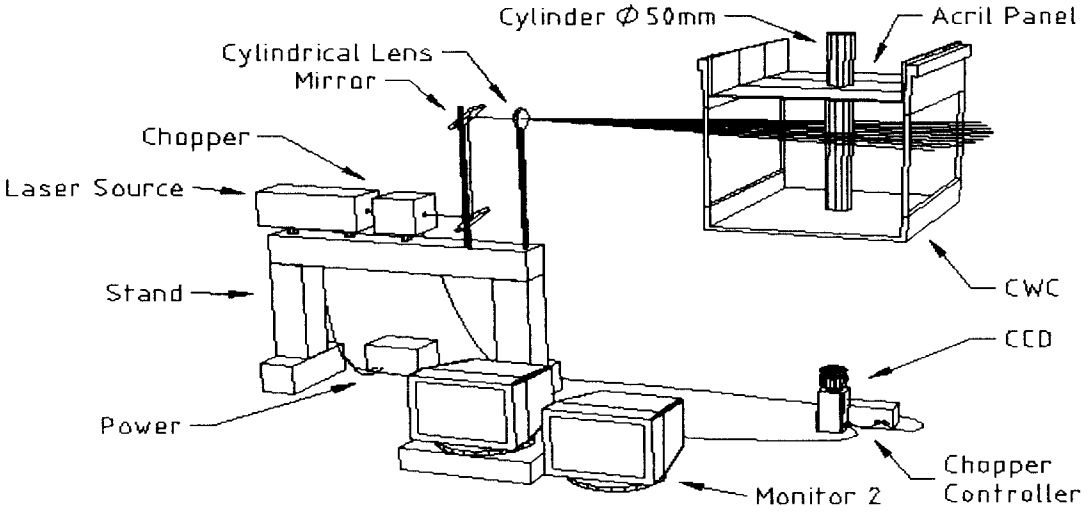

Figure 1 Experimental setup for flow visualization

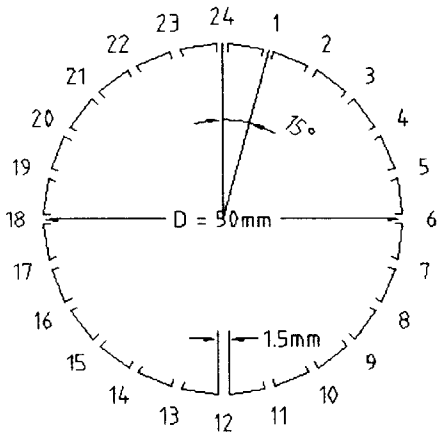

Figure 2 Circular cylinder with 24 pressure taps

with plastic tubes and each pressure is measured consecutively by Validyne pressure transducer with 14cm water head membrane from the number zero tap. The corresponding voltage signal was stored for 10 seconds at 500 Hz sampling rate and averaged for 0.03 sec.

2.2 RESULTS AND DISCUSSIONS

The experimented velocities are summarized in Table 1 with other integrated variables. Due to limitations in speed control the velocity variation seems less systematic but we tried to make the higher velocities double of the lower.

Figure 3 shows one typical flow visualization captured at Reynolds number 4850 along with the picture of the mesh lines drawn with 5cm apart each other for reference. These pictures were automatically taken at a rate of 4 frames per second so we can easily miss the instances that might be more interesting such as moments of maximum or minimum lift. The first and second pictures believed to be for the instances of maximum and minimum lift respectively. At the top a considerable vortex is developed near the upper part of the cylinder and this vortex pulls the real flow down. We can expect a significant acceleration of the flow due to this vortex and consequently maximum lift can occur. The lower is almost opposite of the upper and the fluctuating wake field is well captured. In the shown pictures it is very difficult to point out separation points, however it can be roughly said that the separation occurs a little ahead of the cylinder center and this argument will be

clear with the measured pressure variations later.

Table 1 Summary of experiment and calculation

CWC Freq(Hz)	U (m/s)	Re	C_{DF} (Exp)	St (Exp)	St (Cal)	C_D (Cal)	C_L (Cal)
		200			0.196	1.354±0.044	±0.700
		1000			0.232	1.502±0.217	±1.425
5	0.13	4850	0.96	0.20	0.218	1.355±0.236	±1.407
10	0.25	9730	1.11	0.20	0.226	1.217±0.237	±1.455
20	0.51	19500	1.10	0.19	0.241	1.067±0.225	±1.295
40	1.03	39400	1.05	0.18	0.247	0.985±0.185	±1.104

In order to look into the periodic flow pattern more closely, in Figure 4 consecutive images are shown for one period at Reynolds number 39400. Since the light density is relatively low the wake far downstream is not clear but vortex generations and sheddings are nicely captured. The shedding frequency varies according to the flow speed, which will be discussed later, but the overall flow pattern is nearly independent of the Reynolds number in our range.

In Figure 5 dimensionless measured pressure ($C_p = 2p/\rho U^2$) is plotted. The patterns are not much different for different speeds except that at Reynolds number 4850 (5Hz) the pressure in the wake zone is a little higher than those of others. Noting the pressure starts deviating from the well known potential results between holes 5 and 6 and recalling hole number 6 corresponds to the cylinder center we can speculate that the separation occurs a little ahead of the cylinder center for all cases. Based on this, although far wake seems rather turbulent as seen in the visualized images, the velocity range we are investigating is not high enough for the separation point to be pushed back.

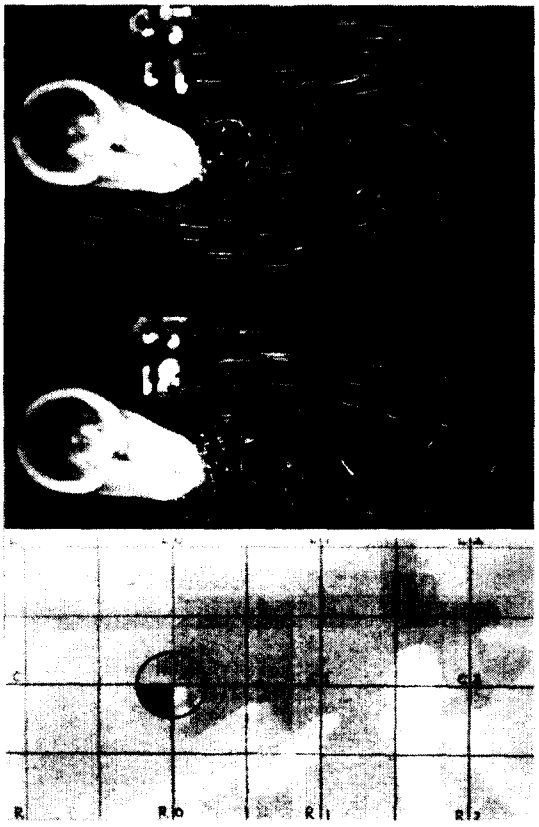

Figure 3 Visualized flow patterns at maximum and minimum lift for Re=4850 along with the mesh

In order to have a rough idea of the fluctuating pressure field we performed FFT for each measured pressure and the results are shown in Figure 6 for hole number 6 which is most informative. While there is not much information is contained at the lowest speed except the two peaks near 4Hz (which are verified to be related to the CWC impeller frequency), at higher speeds there are prominent frequencies at which a considerable amount of amplitude exists. These frequencies are obviously related to the vortex shedding frequencies (roughly 1.0, 2.0 and 4.0) and they are used to evaluate the Strouhal numbers. In Table 1 all the integrated and

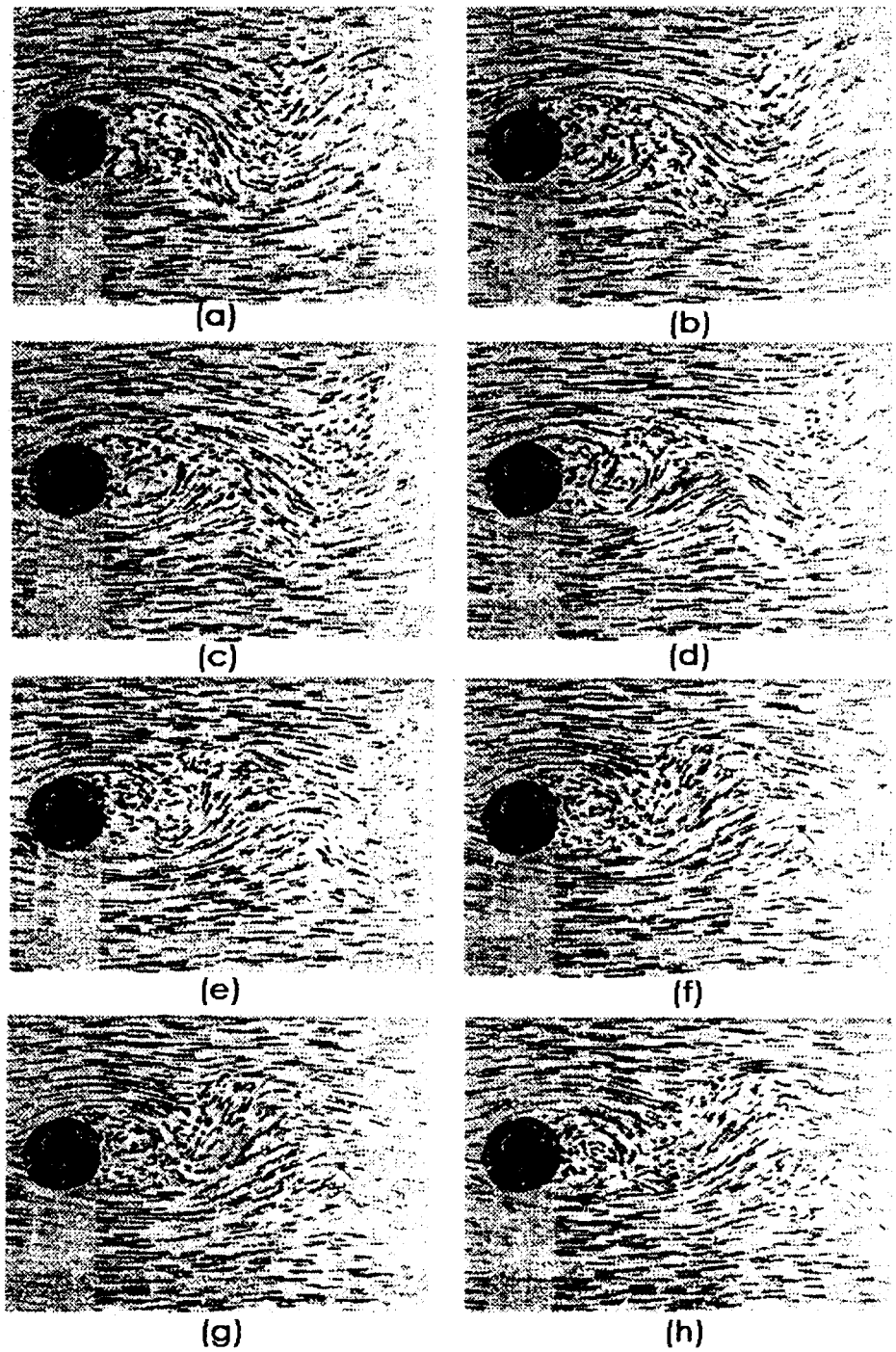

Figure 4 Consecutive flow patterns for one period at Re=39400. Time increases left to right and top from bottom

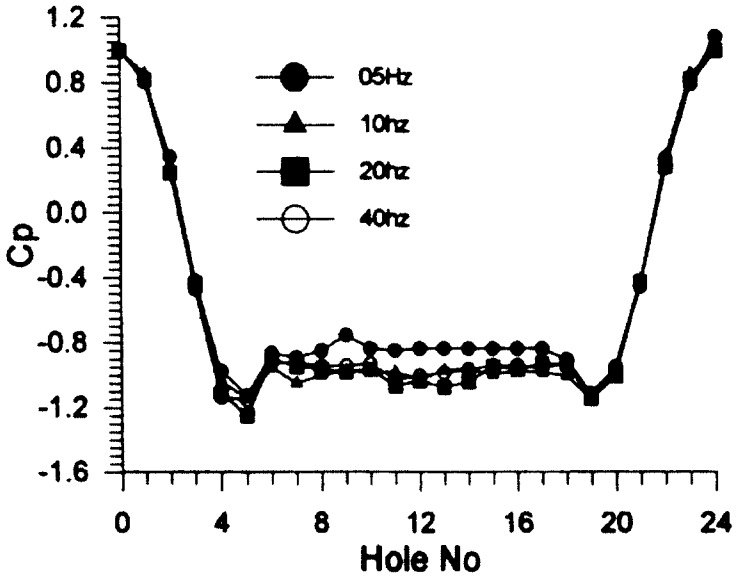

Figure 5 Measured pressure coefficients at different Reynolds numbers

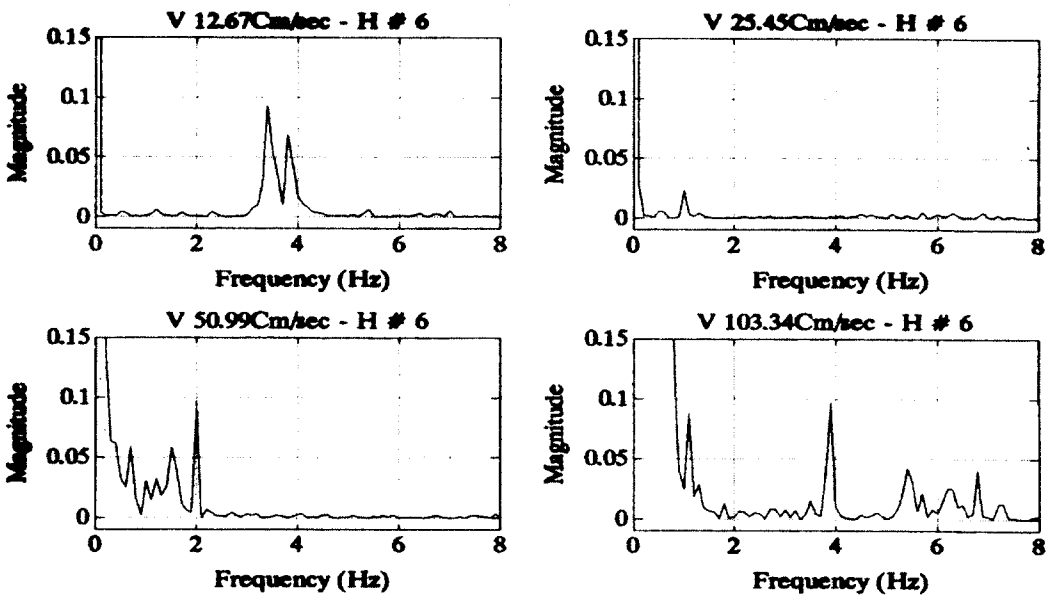

Figure 6 FFT results of the measured pressures at hole 6

evaluated variables are summarized. The pressure drag coefficient is lowest at Reynolds number 4850 and decreases once after it reaches 1.11 at Reynolds number 9730. Although the coefficient excludes viscous stress this pattern agrees with what we all know (see White[1994] for example). The Strouhal number varies a little according to the Reynolds number variation but it almost stays at 0.2.

3. NUMERICAL SIMULATIONS

3.1 FORMULATION AND SOLUTION METHOD

Basically we use quite standard finite difference method so the formulation and the solution method are very briefly summarized and the details can be found in Kim[1994]. Consider the equations of fluid motion in Cartesian coordinates (x, y, z) for unsteady, laminar flow of an incompressible fluid, then the continuity and the momentum equations in dimensionless form are as follows.

$$\frac{\partial u_k}{\partial x_k} = 0 , \tag{1}$$

$$\frac{\partial u_i}{\partial t} + u_j \frac{\partial u_i}{\partial x_j} = -\frac{\partial p}{\partial x_i} + \frac{1}{Re} \nabla^2 u_i \tag{2}$$

For non-dimensionalization cylinder diameter, inflow velocity and fluid density are used. With a body-fitted coordinate system determined, the above equations are transformed into those in the computational domain(ξ, η, ζ) as follows.

$$\frac{1}{J} \frac{\partial}{\partial \xi^m} (JU^m) = \frac{1}{J} \frac{\partial}{\partial \xi^m} (b_i^m u_i) = 0, \tag{3}$$

$$\frac{\partial u_i}{\partial t} + U^k \frac{\partial u_i}{\partial \xi^k} = -\frac{1}{J} b_i^k \frac{\partial p}{\partial \xi^k} + \frac{1}{Re} \nabla^2 u_i \tag{4}$$

where $U^k = b_i^k u_i / J$.

The convection terms in the above equations are discretized by using the so-called "upwind scheme" with 3rd order biased forms and the diffusion terms are central-differenced. The 2nd order implicit method is applied for the time integration after local linearization of convection coefficients.

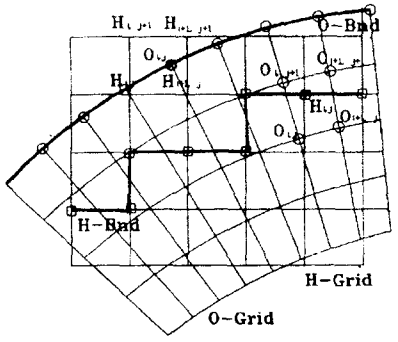

Figure 7 Composite overlaying grids

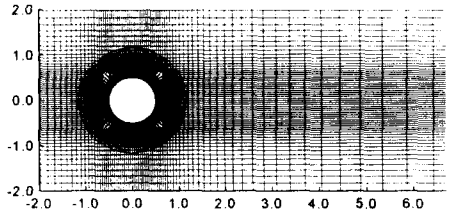

Figure 8 Partial view of a typical grid configuration

In order to evaluate the pressure which is required to update the velocity information the pressure-Poisson equation is solved with pseudo-time iteration including artificial time derivative term, and once the solution converges the pressure field guarantees divergence-free velocity field. Also to deal with so called "checker-board" problem associated with the two consecutive 2nd order central differences of one-interval we introduce a fourth order artificial dissipation following Sotiropoulos et al.[1994] and ADI method is used for the converged solution.

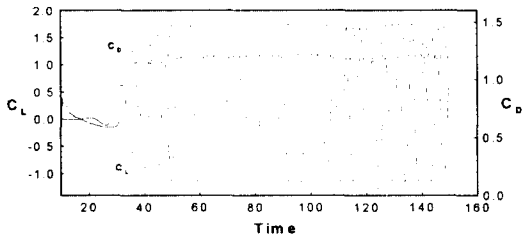

Figure 9 Calculated time history of the drag and lift coefficient at Re=1000

As mentioned earlier we composed two different types of grid; H-type grid and O-type grid (Chesshire et al.[1990], Malmliden[1994]). As shown in Figure 7 overlaying region becomes boundaries of each grid system. For H-grid, which was used for outer region of the flow field, the uniform flow is specified at the inlet and the downstream velocities are extrapolated. Along the branch cut of the inner grid four grid points (two points from each side) are overlapped to ensure the continuous change of flow variables and no slip condition is applied to the cylinder surface. In the overlaying regions of H-and O-grid a bilinear interpolation is used from one grid to the other and those interpolated values are used as boundary conditions. Figure 8 is a partial view of the grid system. For most of the calculations 82 by 43 and 111 by 91 grid points were used for O-and H-grid, respectively. The block iterations are performed 3 to 6 times and 0.05 or 0.01 is used as the time increment. As an initial condition potential solution corrected by the Blasius boundary layer solution was used.

3.2 RESULTS AND DISCUSSIONS

The numerical methods described in the previous section were applied to simulate the flow around a circular cylinder. Cases of Reynolds numbers corresponding to those from the experiments were calculated and cases of Reynolds numbers 200 and 1000 were also calculated to compare our results with previous investigations.

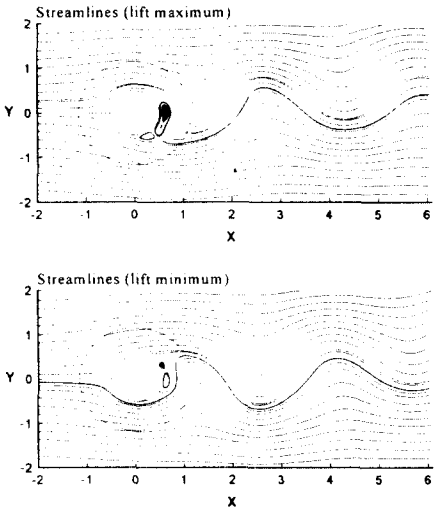

Figure 10 Calculated streamlines at maximum and minimum lift for Re=19500

In Figure 9 a typical time history of the drag and lift coefficient during the calculation is shown. For the first several hundreds iterations time accurate solution was not sought but once the solution becomes periodic the oscillating drag and lift shows a steady mean. The periodicity of coefficients implies the time accuracy of the present method. The Strouhal numbers and drag/lift coefficients calculated are summarized also in Table 1. While at lower Reynolds number (Re=200) the results agree very well with previous experiments (C_D=1.3 from Wille[1960], St=0.19 from Kovasznay[1949]) but at higher Reynolds numbers we believe that an improvement in accuracy is necessary (drags are overpredicted). We realized that the results with different values of numerical controlling parameters such as time increment were varied

but an intensive investigation on such effects was not enough.

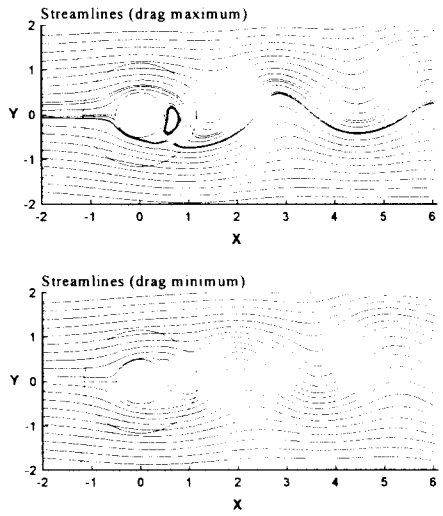

Figure 11 Calculated streamlines at maximum and minimum drag for Re=19500

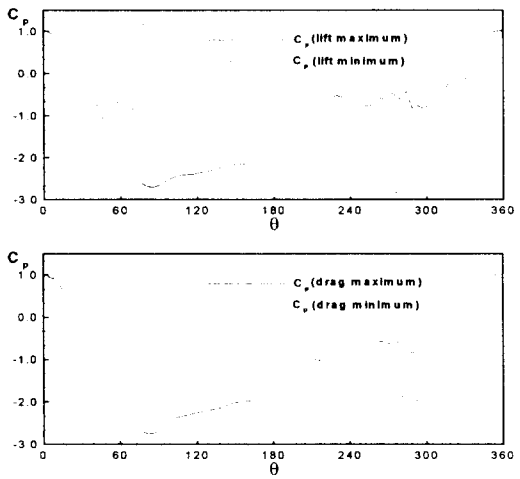

Figure 12 Calculated pressure coefficient along the circumference at maximum and minimum lift for Re=19500

Flow patterns at the time of maximum and minimum lift are shown in Figure 10 for Re=19500 as streamlines. As discussed in the experiments well developed vortices about to leave the cylinder are shown at the upper and lower part of the cylinder causing the maximum and minimum lift respectively and they are distorting the downstream flow field significantly. Consecutively separated vortices construct fluctuating downstream flow field and the two pictures show a good symmetry about the y=0 axis implying a reasonable capability of the present method to capture unsteadiness.

In Figure 11 similar flow patterns are shown at the instances of maximum and minimum drag. Comparing with Figure 10 the maximum drag nearly coincides with maximum or minimum lift while the minimum drag has a phase difference. As easily can be understood the period of the drag oscillation is one half of that of lift oscillation (also can be seen in Figure 9) and the lowest drag occurs when a new vortex starts growing (see the bottom picture of Figure 11). As shown in Figures 12 and 13, the pressure distributions in the wake at maximum drag and maximum (or minimum) lift are similarly

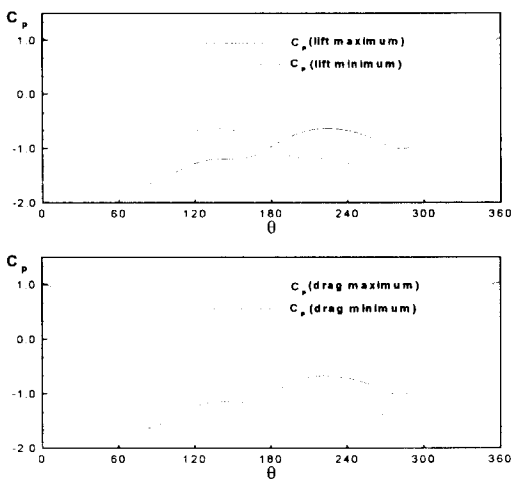

Figure 13 Calculated pressure coefficient along the circumference at maximum and minimum lift for Re=200

asymmetric about the y=0 axis while at minimum drag the pressure in the wake is rather uniform.

4. SUMMARY

The flow around a circular cylinder is investigated both experimentally and numerically. The experiment performed in a circulating water channel facility includes pressure measurements at 24 locations along the circumference of the cylinder and flow visualizations by using laser sheet. The Reynolds number ranges from 4800 to 40000. Also a numerical method was developed to solve the Navier-Stokes equations for unsteady laminar flows around the circular cylinder. The present method used the finite-difference scheme in the collocated grid system and the pressure-Poisson method was employed to obtain divergence-free velocity field at each time step. For an efficient grid distribution a composite griding with H- and O-type grids was used.

Vortex sheddings are nicely captured both in experiments and calculations and the integrated values are quite comparable. Visualized flow patterns are believed to be quite helpful to understand the overall picture of the flow but, in order to become more informative, problems associated with synchronization and resolution should be reconsidered. Composite overlaying grid was efficiently used without a significant accuracy loss and, on the whole, our numerical method predicted the flow field well. Maximum drag occurs nearly when the lift is maximum (or minimum) but the minimum drag occurs when attached vortices start growing so the lift is rather close to zero.

ACKNOWLEDGEMENT

This work has been supported by KOSEF under the contract no. 94-0200-03-01-3.

REFERENCES

1) Bruce, T., Easson, W.J. and Greated, C.A., "The kinematics of oscillatory flows past cylindrical structures", Proc. 3rd ISOPE, Singapore, 1993
2) Chesshire, G. and Henshaw, W.D., "Composite overlapping Meshes for the solution of partial differential equations", JCP, Vol.90, 1990
3) Faltinsen, O.M., Sea loads on ships and offshore structures, Cambridge, 1990
4) Faltinsen, O.M., "Sea loads on floating offshore systems", OTC, Houston, USA, 1993
5) Hu, C. and Koterayama, W., "A numerical experiment on slow drift damping forces of an ocean structure", Proc. 2nd Japan-Korean Joint Workshop on Ship and Marine Hydrodynamics, Osaka, Japan, 1993
6) Kim, W.J., An Experimental and Computation Study on the Pressure Distribution around a Hydrofoil Moving under the Free Surface, Report UCE554-1845D, KRISO, 1994
7) Kovasznay, L.S.G., "Hot-wire Investigation for the Wake behind Cylinders at Low Reynolds Numbers," Proc. Roy. Soc. A, Vol. 198, pp. 174-190, 1949
8) Malmliden, J.F., "Development of numerical methods for ship flow using composite overlapping grids", Ph.D. Dissertation, Royal Institute of Technology, 1994
9) Rosenfeld, M., Kwak, D., Vinokur, M., "A Solution Method for the Unsteady and Incompressible Navier-Stokes Equations in generalized Coordinate Systems," AIAA-Paper 88-0718, 1988
10) Rosenfeld, M., Kwak, D., Vinokur, M., "A Fractional Step Method for the Unsteady for the Unsteady and Incompressible Navier-

Stokes Equations in generalized Coordinate Systems," Journal of Computational Physics, Vol. 94, pp. 102-137, 1991

11) Sibetheros, I.A. and Miksad, R.W., "An experimental investigation of the near flow around a cylinder in reversing planar flow", Proc. 3rd ISOPE, Singapore, 1993

12) Sotiropoulos, F., Kim, W.J., Patel V.C. , "A Computational Comparison of Two Incompressible Navier-Stokes Solvers in Three-Dimensional Laminar Flows," Computers and Fluids, Vol. 23, No. 4, pp.627-646, 1994

13) Suhara, T., Koterayama, W., Tasai, F. and Watanabe, K., "Behavior and Tension of oscillating chain in water", Proc. SNAJ, 1981

14) Suhara, T., Koterayama, W., Hiyami, H. and Koga, Y., "Behavior and Tension of oscillating chain in water(II)", Proc. SNAJ, 1983

15) Suhara, T., Koterayama, W., Hiyami, H. and Koga, Y., "Behavior and Tension of oscillating chain in water(III)", Proc. SNAJ, 1984

16) White, F.M., Fluid Mechanics, McGraw-Hill, New York, 1994

17) Wille, R., "Karman Vortex Streets," Adv. Appl. Mech., Vol. 6, pp. 273, 1960